

Controlled Chemistry via Contactless Manipulation and Merging of Droplets in an Acoustic Levitator

Stephen J. Brotton and Ralf I. Kaiser*

Cite This: *Anal. Chem.* 2020, 92, 8371–8377

Read Online

ACCESS |



Metrics & More



Article Recommendations



Supporting Information

ABSTRACT: A unique, versatile, and material-independent approach to manipulate contactlessly and merge two chemically distinct droplets suspended in an acoustic levitator is reported. Large-amplitude axial oscillations are induced in the top droplet by low-frequency amplitude modulation of the ultrasonic carrier wave, which causes the top sample to merge with the sample in the pressure minimum below. The levitator is enclosed within a pressure-compatible process chamber to enable control of the environmental conditions. The merging technique permits precise control of the substances affecting the chemical reactions, the sample temperature, the volumes of the liquid reactants down to the picoliter range, and the mixing locations in space and time. The performance of this approach is demonstrated by merging droplets of water (H₂O) and ethanol (C₂H₅OH), conducting an acid–base reaction between aqueous droplets of sodium hydroxycarbonate (NaHCO₃) and acetic acid (CH₃COOH), the hypergolic explosion produced via merging a droplet of an ionic liquid with nitric acid (HNO₃), and the coalescence of a solid particle (CuSO₄·5H₂O) and a water droplet followed by dehydration using a carbon dioxide laser. The physical and chemical changes produced by the merging are traced in real time via complementary Raman, Fourier-transform infrared, and ultraviolet–visible spectroscopies. The concept of the contactless manipulation of liquid droplets and solid particles may fundamentally change how scientists control and study chemical reactions relevant to, for example, combustion systems, material sciences, medicinal chemistry, planetary sciences, and biochemistry.



The control and merging of two droplets is fundamentally important to unravel not only basic physical processes such as mixing dynamics¹ and intermolecular forces,² but more importantly the outcome of chemical reactions occurring in liquids, combustion processes,³ material sciences,⁴ and biochemistry.^{4,5} Contemporary devices of contactless processing exploit tandem electrodynamic traps,⁶ guided droplet collisions combined with branched quadrupole traps,⁷ optical trapping (or laser tweezers),⁸ and diamagnetic levitation.⁹ However, the electric, magnetic, and laser traps lack versatility for chemical applications, since these techniques are sensitive to specific physical properties of the samples such as the electric charge (electrodynamic traps), magnetic permeability (diamagnetic traps), and the refractive index (laser traps).

In acoustic levitation, an object is suspended in a gaseous medium by acoustic radiation pressure.^{10–12} The acoustic force is independent of the electric and magnetic properties of the sample and, therefore, enables a wider range of substances to be studied than via the aforementioned electromagnetic traps. Levitation has the advantage of avoiding the complicating effects of a contacting surface and so permits the so-called “containerless processing” of a single, levitated particle. Acoustic levitation has been used to process containerlessly individual particles and single droplets.^{5,13–17} To extend the

acoustic technique to the transport and coalescence of levitated droplets, ultrasonic phased arrays consisting of a chessboard-type arrangement of piezoelectric transducers have been developed that horizontally transport and merge matter by the spatial and temporal modulation of the acoustic field.^{1,18,19} However, the complex design and size make these acoustophoretic devices less suitable for operation within a chemical process chamber at controllable temperatures, and reduces the accessibility for the multiple, complementary spectroscopic probes required to trace the chemical reactions after merging the two droplets. Within a single-axis acoustic levitator, Bjelobrck et al.²⁰ united two droplets in air by merging two pressure nodes into one by varying the distance between the transducer and reflector, but the change in radiation pressure during the droplet movement adversely affects the acoustic

Received: March 1, 2020

Accepted: May 13, 2020

Published: June 1, 2020



resonance condition which can lead to disintegration of the droplets.

Thus, although significant progress has been made in the methods of droplet transport and coalescence, the application of a merging technique to solve the realistic problems encountered in chemical and biological research has yet to be achieved. In particular, a versatile technique employing the contactless manipulation of liquids to control and merge two chemically distinct droplets and simultaneously follow the resulting reactions via a complementary set of spectroscopic probes has not been accomplished to date. To address the requirement, we report on a versatile approach to merge two droplets levitated in a single-axis device by the low-frequency modulation of the ultrasonic carrier wave (Figure 1). By

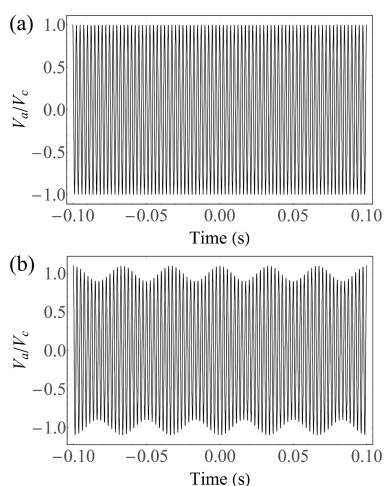


Figure 1. Schematic representation of the (a) unmodulated and (b) modulated voltages applied to the piezoelectric transducer.

preparing two chemically distinct droplets in adjacent pressure nodes, this technique enables the droplets to be merged and the chemical reactions within the merged droplet followed via complementary infrared, Raman, and ultraviolet–visible (UV–vis) spectroscopies. By implementing this levitation device within a pressure-compatible process chamber interfaced to a carbon dioxide laser, the reactions of samples including toxic liquids can be explored in a controlled environment over extended temperature ranges. The experimental set up permits precise control of the substances affecting the chemical reactions, the sample temperature, and the volumes of the liquid reactants down to the picoliter range. Furthermore, since the two merging droplets mix rapidly at a precise location in space and time, any measurement involving chemical kinetics, such as determining the ignition time of a hypergolic reaction (Results and Discussion), can be measured more accurately. The unique performance of this approach is demonstrated by merging droplets of water (H_2O) and ethanol ($\text{C}_2\text{H}_5\text{OH}$), conducting an acid–base reaction between aqueous droplets of sodium hydroxycarbonate (NaHCO_3) and acetic acid (CH_3COOH), by reacting a droplet of the hypergolic ionic liquid 1-butyl-3-methylimidazolium dicyanamide ([BMIM][DCA]) with nitric acid (HNO_3), and coalescing a solid particle ($\text{CuSO}_4 \cdot 5\text{H}_2\text{O}$) and a water droplet followed by dehydration of the water–copper sulfate solution using a carbon dioxide laser. These studies represent benchmarks for physical mixing processes, reactions in aqueous solution, unravelling the oxidation of toxic ionic liquids, and liquid–

solid interactions. The reaction between a droplet of [BMIM][DCA] and nitric acid is discussed in the Results and Discussion section; full details of the three other experiments are presented in the Supporting Information.

EXPERIMENTAL METHODS

Levigator Experimental Apparatus. The levigator experimental apparatus has been discussed in detail previously.^{14,16} In the acoustic levigator, ultrasonic sound waves with a frequency of 58 kHz are produced by a piezoelectric transducer and reflect from a concave plate to generate a standing wave.¹⁴ The sound waves produce acoustic radiation pressure,^{10,21} which levitate a sample slightly below one of the pressure minima of the standing wave. The distance between the transducer and reflector is set to 2.5 wavelengths (or 14.8 mm) producing five pressure nodes, although only the second and third pressure nodes above the ultrasonic transducer are suitable for levitation. The largest diameter of droplets or particles that can be levitated in the present apparatus is approximately 3 mm, whereas the smallest is around 15 μm . In the experiments discussed below, before merging the oblate spheroidal droplets have horizontal and vertical diameters in the ranges of 2.0–2.8 mm and 1.2–1.6 mm, respectively.

The levigator is enclosed within a pressure-compatible process chamber to permit levitation in an inert gas or a highly reactive gas to investigate chemical reactions. In the present experiments, the chamber was filled with argon at the temperature and pressure of 298 K and 880 Torr, respectively. To levitate chemically distinct droplets in adjacent pressure nodes, two syringes are attached to an outside port on the chamber. Each syringe is connected via chemically inert polyetheretherketone (PEEK) tubing to one of two micro-needles inside the chamber. The pair of needles is attached to the end of a wobble stick, which permits either needle tip to be positioned within the second or third pressure minimum to deposit a droplet before being withdrawn prior to the experiments. To levitate a liquid droplet and a solid particle, one of the needles was replaced by a wire-mesh spatula. The levitated droplet can be heated to the desired temperature by varying the output power of a 40 W, Synrad Firestar v40 laser emitting at the wavelength of 10.6 μm . The temperature of the levitated sample was measured by an FLIR A6703sc thermal-imaging camera.

The process chamber is surrounded by complementary Raman, FTIR, and UV–vis spectrometers to identify any chemical or physical modifications of the levitated sample. In the Raman spectrometer system, a diode-pumped, Q-switched Nd:YAG laser emits a 532 nm beam which is focused by a lens onto the sample. The Raman-shifted, backscattered photons are focused by a camera lens into a HoloSpec *f*/1.8 holographic imaging spectrograph, where two overlaid holographic transmission gratings disperse the spectrum across a CCD camera (Princeton Instruments PI-Max 2 ICCD) and simultaneously cover the Raman-shift ranges from 300–2450 cm^{-1} and 2400–4400 cm^{-1} with a resolution of 9 cm^{-1} . Infrared transmission spectra in the 4000 to 400 cm^{-1} wavenumber range can be obtained using mirror optics to focus the output from a Thermo Scientific Nicolet 6700 FTIR spectrometer into a diameter of 4 mm around the levitated sample before recollimating the infrared beam prior to detection. Any part of the IR beam incident on the sample is either absorbed or scattered away from the detector, so that only gases in the region of the droplet are detected by transmission FTIR

spectroscopy. The number density of the absorber, n , and, hence, the moles of gases produced in the process chamber can be calculated using the Beer–Lambert law:²²

$$n = \frac{A \log_e 10}{\sigma L} \quad (1)$$

where A is the absorbance from our spectrum, σ is the reference absorption cross section from the HITRAN database,²³ and L is the path length of 37.6 cm.

In the UV–vis spectrometer, the output from a UV–vis source is transmitted via a fiber-optic feedthrough within a conflat flange to seven, 400 μm illumination fibers of a Y-type reflectance probe located inside of the process chamber. The radiation backscattered from the levitated sample is collected by one 600 μm diameter read fiber, exits the chamber by the conflat fiber-optic feedthrough, and lastly goes into a StellarNet SILVER-Nova UV–vis spectrometer, which operates in the 200 to 1100 nm wavelength range at a resolution of 2 nm. To film high-speed events, a Phantom Miro 3a10 camera combined with a Navitar Zoom 6000 modular lens system was aligned on the levitated sample via an optical viewport.

The reaction rate constants can be determined by analyzing the growth curves for formation of the new peaks or the decay curves for the reduction of the unreacted peaks in a sequence of the Raman spectra recorded as a function of time. Such an approach has previously been applied to deduce the reaction rates for the oxidation of a levitated droplet of an energetic ionic liquid by nitrogen dioxide.¹⁶ The fastest reaction rates that can be followed are ultimately limited by the minimum times to collect a single Raman, FTIR, or UV–vis spectrum of 0.25 s, 1 s, and 0.001 s, respectively.

Droplet Oscillations. To induce oscillations in the droplet, the voltage of the carrier wave is amplitude modulated by a low-frequency voltage output from a signal generator. The voltage V_a applied to the ultrasonic transducer is given by

$$V_a = V_c(1 + m \sin \omega_m t) \sin \omega_c t \quad (2)$$

where V_c and ω_c are the voltage amplitude and angular frequency ($\omega_c/2\pi = 58$ kHz) of the unmodulated ultrasonic standing wave, respectively; ω_m is the angular frequency of the modulation voltage with typical values in the range of $20 \lesssim \omega_m/2\pi \lesssim 40$ Hz; and m is the modulation index (Figure 1). The resulting axial acoustic radiation pressure, $P_r(z, t)$, is given by (Supporting Information):

$$P_r(z, t) \approx -\frac{A^2}{4\rho_0 c_0^2} \cos 2k_z z (1 + 2m \sin \omega_m t) \quad (3)$$

where A is the pressure amplitude of the standing wave, ρ_0 is the ambient density, c_0 is the speed of sound, z is the displacement from the central pressure minimum along the central axis of the levitator, and $k_z = \omega_c/c_0$ is the wavenumber of the ultrasonic wave. The integral of the time-independent pressure term $\propto -A^2 \cos 2k_z z$ over the surface of the sample produces a net upward axial levitation force that compensates the downward force of gravity. The time-varying axial force arising from the term $\propto -A^2 m \cos 2k_z z \sin \omega_m t$ causes the droplet to be periodically compressed at the poles into an oblate shape and subsequently elongated into a prolate shape along the vertical axis. The surface tension of the droplet provides a restoring force. The droplet may thus be driven into oscillations if the modulation frequency ω_m is similar to that for one of the resonant modes. For the axisymmetric

vibrational modes relevant here, the vibrational frequencies can be analyzed by first expanding the radius $r(\theta, t)$ of the deformed droplet as a series of Legendre polynomials:

$$r(\theta, t) = r_0 \left[1 + \sum_{l=2}^{l_{\max}} c_l(t) P_l(\cos \theta) \right] \quad (4)$$

where r_0 is the radius of a spherical droplet with the same volume. An expression for the frequencies f_l of the axisymmetric vibrational modes was derived by Rayleigh:²⁴

$$f_l = \frac{1}{2\pi} \sqrt{\frac{\sigma}{\rho r_0^3} l(l-1)(l+2)} \quad (5)$$

where σ is the surface tension and ρ is the density of the droplet. Equation 5 was derived for vibrations about a spherical droplet, but the analysis remains approximately valid for oscillations around the oblate equilibrium shape typical of a levitated droplet if r_0 is replaced by the equatorial radius a .²⁵ As examples of axisymmetric modes, we show the lowest mode with $l = 2$ or the quadrupole mode in Figure 2; the $l = 3$ and $l =$

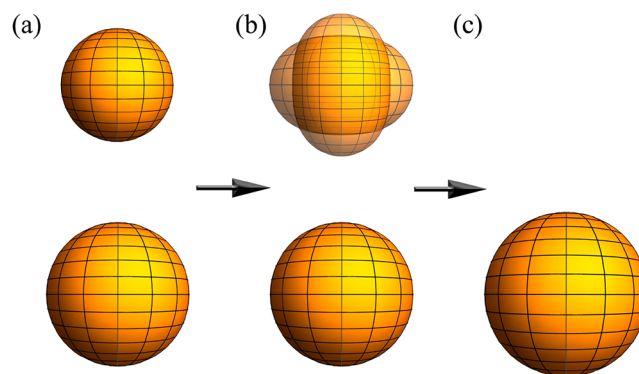


Figure 2. Pictorial representation of the droplet merging procedure showing (a) two droplets levitated in adjacent pressure nodes before modulation, (b) the oblate and prolate axial shapes induced in the upper droplet when oscillating in the quadrupole mode, and (c) the merged droplet.

6 modes are displayed in Figure S3. Experimental studies for the driven oscillations of droplets reveal that pure modes with one value of l can be selectively excited, but mixed modes, for example $l = 3$ and $l = 6$, can also form by intermode energy transfer and these resemble the highly-excited droplet shapes immediately before merging.²⁶

For small amplitude oscillations, experimental measurements for the resonance frequencies of the first four modes were found to be in approximate agreement with theoretical predictions.²⁷ In particular, the resonant frequency of the fundamental $l = 2$ mode varied with the radius r_0 according to $f_l \propto r_0^{-1.5}$ consistently with eq 5. Extension of the measurements to large-amplitude driven oscillations showed, however, that the resonance frequency increased slightly relative to eq 5 as the droplet was deformed into an increasingly oblate shape.²⁸ Nonaxisymmetric oscillations of acoustically levitated water droplets excited by a similar modulation technique have been observed experimentally.²⁵

Merging Approach. First, one droplet was levitated in the second pressure minimum above the ultrasonic transducer and then the other droplet dispensed with a smaller diameter into the pressure minimum above. Second, the modulation

frequency f_m was tuned to match the resonant frequency of the upper droplet, and hence axial oscillations of the fundamental $l = 2$ mode were induced. The oscillations induced were smaller in the lower droplet because the resonant frequency depends on the droplet radius r_0 via eq 5. Third, the modulation voltage was gradually increased to cause the amplitude of the induced oscillations to grow. For large amplitudes, the droplet often appeared to oscillate in a non-normal mode, although the vibrations were probably a combination of several pure modes, as discussed above, including nonsymmetric geometries.²⁸ Fourth, when the oscillation amplitude exceeded the dimensions of the trapping acoustic potential well, the top droplet fell under gravity into the pressure minimum below, guided by the horizontal restoring force produced by the radial acoustic Bernoulli stress²⁹ and the curved reflector, where it merged with the lower droplet. Lierke suggested a different approach for the contactless merging of droplets by inducing radial sample oscillations within a slightly tilted levitator,³⁰ as described by the parametric Mathieu equation.³¹ The oscillation of a droplet was damped by the viscosity of the liquid and the dragging effect of the surrounding gas. Consequently, the Q -factor of the resonance was reduced, and hence the droplet oscillated for a range of frequencies around the central value, f_1 (eq 5).^{27,28} Two droplets with only slightly different radii can therefore both be set into oscillation by the modulated ultrasonic wave, as was often observed in the present experiments. The top droplet will, nevertheless, escape from the acoustic potential well first even if its oscillation amplitude is only slightly larger than that for the droplet below. We have focused on merging droplets with diameters near the upper limit of 3 mm (see the Levitator Experimental Apparatus section), since the probability of the two particles colliding and, hence, merging reduces as the diameter approaches the lower limit of 15 μm . The merging technique could, in principle, be extended to smaller droplets by reducing the wavelength of the acoustic standing wave.

RESULTS AND DISCUSSION

A hypergolic propellant consists of a fuel and an oxidizer, which spontaneously ignite upon mutual contact. The most commonly employed hypergolic propellant is composed of a dinitrogen tetroxide (N_2O_4) oxidizer and hydrazine (N_2H_4) fuel.^{32,33} Hydrazine has critical shortcomings, however, including toxicity, an inherently high vapor pressure, and corrosiveness.³² Several ionic liquids (ILs) have been found to be hypergolic with common oxidizers,^{34–38} for example, 1-butyl-3-methylimidazolium dicyanamide ([BMIM][DCA]) (Figure S1) and white-fuming nitric acid (WFNA).³⁹ Owing to suitable physical properties of ionic liquids such as the melting point, energy density, and viscosity and the potential to tune these properties by selecting different anion and cation combinations,⁴⁰ there has been intensive research to develop ionic-liquid-based hypergolic fuels that avoid the disadvantages of hydrazine-based propellants.^{34–38} The two-droplet merging technique coupled with the complementary spectroscopic probes interfaced to the levitator apparatus is an ideal set up to perform such hypergolic ignition studies and explore the underlying chemistry. Since [BMIM][DCA] and WFNA ignite upon mutual contact and produce intense flames,⁴¹ to acoustically trap the merged droplet for the spectroscopic investigation we reduced the reaction rate and the explosiveness of the system by using diluted, 70% nitric acid (HNO_3).

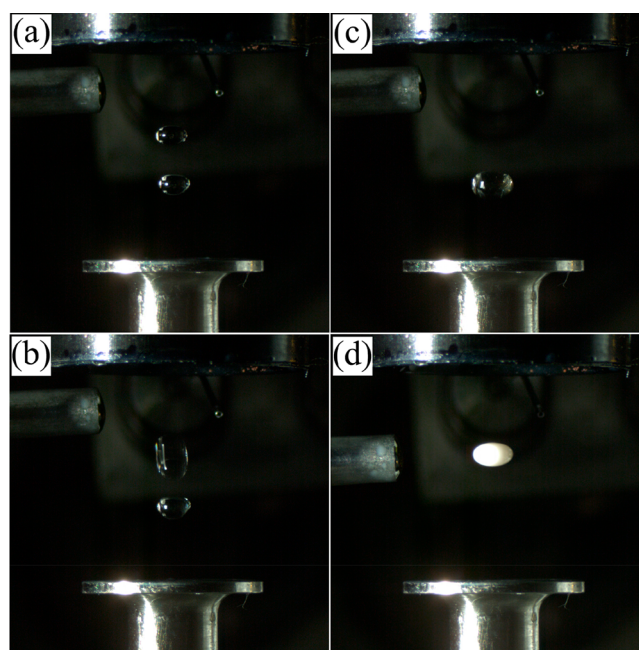


Figure 3. (a) Droplet of nitric acid levitated above a [BMIM][DCA] droplet, (b) the axial oscillations induced in the upper droplet, (c) the merged droplet before significant reaction, and (d) the merged droplet captured in an upper pressure node following the chemical reaction. The droplet merging process is shown in Movie S1 (Supporting Information).

Photographs of the nitric acid droplet levitated above the [BMIM][DCA] droplet and the merged droplet are displayed in Figure 3. The nitric acid, [BMIM][DCA], and merged droplets are oblate spheroids with dimensions of 2.1 mm \times 1.3 mm, 2.1 mm \times 1.4 mm, and 2.7 mm \times 1.6 mm, respectively. A film of the merging reaction is shown in Movie S1. Immediately after the merging, the products released into the gas phase were rapidly ejected from the lower side of the droplet which propelled the droplet upward; however, the acoustic trapping potential coupled with gravity remarkably captured the escaping droplet into an upper pressure node. After the gaseous products were released, the shape and location of the droplet stabilized and a white precipitate formed. The Raman spectrometer collects photons back-scattered from the droplet and, hence, traces chemical changes of the droplet itself.¹⁴ In contrast, the FTIR spectrometer system operates in transmission mode,¹⁴ and therefore only gaseous products or molecules vaporized from the surface of the reactants are detected. FTIR spectra of the two droplets before and after coalescence were each acquired for 1 min and are shown in Figure 4. The [BMIM][DCA] spectrum does not contribute to the FTIR spectra owing to the very low vapor pressure of ionic liquids. The Q -branch wavenumbers and vibrational mode assignments for bands $a^*–d^*$ of the nitric acid droplet before the merging are presented in Table S1.⁴² The vibrational modes for bands $a–n$ of the gaseous products are assigned in Table S2 to carbon dioxide (CO_2) [$\nu_3(\sigma_u^+)$ asymmetric stretching mode, 2349 cm^{-1} ; $\nu_2(\pi_u)$ bending mode, 668 cm^{-1}] and nitrous oxide (N_2O) [$\nu_3(\sigma^+)$ N–N stretching, 2223 cm^{-1} ; $\nu_1(\sigma^+)$ N–O stretching mode, 1285 cm^{-1}] in accordance with the following reaction mechanism between the [DCA][−] (or [N(CN)₂][−]) anion and nitric acid:³⁹

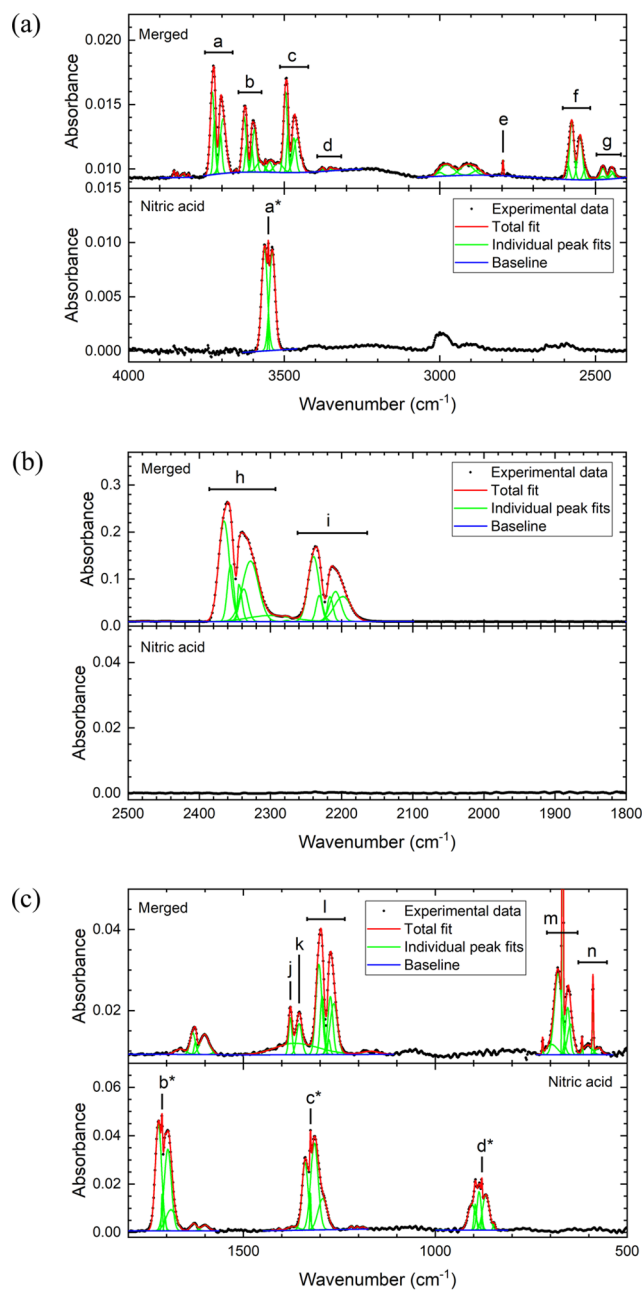
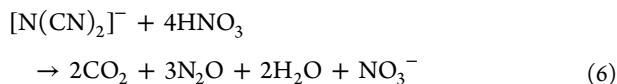


Figure 4. FTIR spectra of the nitric acid droplet and the merged droplet in the (a) 4000–2400 cm^{-1} , (b) 2500–1800 cm^{-1} , and (c) 1800–500 cm^{-1} wavenumber regions. The wavenumbers for the nitric acid bands labeled a^* – d^* are compiled in Table S1; the vibrational modes for the newly formed bands a – n are presented in Table S2.



Raman spectra of the nitric acid, the [BMIM][DCA], and the merged droplets are presented in Figure 5. Each Raman spectrum was acquired for approximately 10 min to achieve a high statistical accuracy. Since nitric acid partly dissociates in aqueous solution to form the nitrate (NO_3^-) and hydronium (H_3O^+) ions, the Raman spectrum for the aqueous nitric acid droplet was identified by comparison with the 10 Raman active vibrational modes of molecular nitric acid and the 5 Raman

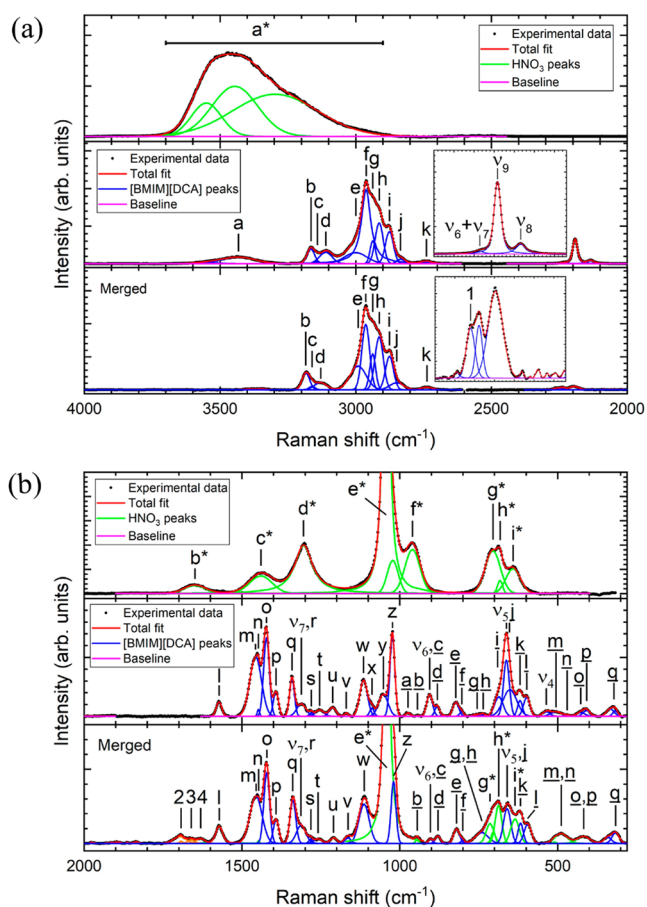


Figure 5. Raman spectra and individual peak fits for nitric acid, [BMIM][DCA], and the merged droplet in the (a) high and (b) low Raman-shift regions. The inserts from 2350–2020 cm^{-1} show the region of the intense [DCA] peaks in detail. The wavenumbers and vibrational mode assignments for the nitric acid, [BMIM][DCA], and the new peaks (1)–(4) are presented in Tables S3, S4, and S5, respectively.

active modes of the nitrate anion (Table S3).^{42,43} For the Raman spectrum of the [BMIM][DCA] droplet, the vibrational modes for the numerous observed peaks are assigned in Table S4 by comparison with the wavenumbers for the 9 normal modes of the $[\text{DCA}]^-$ anion and the 75 normal modes of the $[\text{BMIM}]^+$ cation.¹⁶ Clearly, the Raman spectrum of the merged droplet differs significantly from the spectra of the unreacted nitric acid and [BMIM][DCA] droplets. First, the peaks at 2134, 2191, and 2236 cm^{-1} produced by the asymmetric stretching mode $\nu_{\text{as}}(-\text{C}\equiv\text{N})$, symmetric stretching mode $\nu_{\text{s}}(-\text{C}\equiv\text{N})$, and the $\nu_{\text{s}}(\text{C}-\text{N}) + \nu_{\text{as}}(\text{C}-\text{N})$ combination band of the $[\text{DCA}]^-$ anion, respectively, reduced significantly following the reaction. In contrast, the peaks produced by the $[\text{BMIM}]^+$ cation, such as the structure between 2800 cm^{-1} and 3200 cm^{-1} , are essentially unchanged. Second, a new peak 1 appeared which is assigned to $-\text{C}\equiv\text{N}$ stretches, together with new peaks 2–4 attributed $\text{N}=\text{O}$ stretches of the organic nitrites (Table S5).⁴⁴ The remainder of the merged droplet spectrum is the sum of the unreacted nitric acid and [BMIM][DCA] spectra (Figure 5). Consequently, these data suggest that the $[\text{DCA}]^-$ anion rather than the $[\text{BMIM}]^+$ cation reacted with the nitric acid to produce the carbon dioxide and nitrous oxide gaseous products (reaction 6) detected by the FTIR spectrometer, in addition to the

functional organic groups monitored by Raman spectroscopy and listed in Table S5.

CONCLUSION

We have presented a versatile, original method to merge contactlessly two droplets levitated in adjacent pressure minima of a single-axis acoustic levitator and followed the resulting reactions via complementary Raman, FTIR, and UV–vis spectroscopic probes. To demonstrate the wide range of possible applications, the technique was used to investigate liquid systems relevant to physical mixing, reactions in aqueous solutions, and hypergolic ignition processes, in addition to solid–liquid interactions including dehydration at elevated temperatures. The present approach has the potential for a diverse range of additional fundamental and applied research. For example, laser-heating of the individual or merged droplets will enable reactions to be investigated over an extended temperature range relevant to combustion processes.²² Furthermore, the incorporation of a closed-cycle helium refrigerator or liquid nitrogen-based cooling system would reduce the temperatures of the buffer gas in the process chamber to those found on the planets and their moons, which would help us explore merging processes of astrochemical relevance including of hydrocarbon droplets in hydrocarbon rich atmospheres of planets and their moons such as Titan.⁴⁵ The possibility of mixing without biological contamination or a loss of reagents owing to contact with supports makes our approach suitable for biological applications, such as studying DNA transfection in which small volumes of biological suspensions of living mammalian cells are merged with plasmids.⁴⁶ The ability to collect high-sensitivity, time-dependent spectroscopic data from samples with volumes of only a few picoliters also makes the method highly suitable to study infections in biological tissues, such as single blood drops, where limited material is available and follow the biochemical kinetics, thus utilizing levitated droplets as wall-less test tubes.⁴⁷ By merging samples such as aqueous sulfates, nitric acid, or hydrocarbons, the controlled environment of the levitator would also be ideal to simulate the collisions and coagulation of aerosol particles occurring in Earth's atmosphere and, hence, understand the key chemical reactions previously accessible only under bulk conditions.⁴⁸ The concept of contactless merging thus opens new avenues of chemistry, material science, medical chemistry, and biology to explore.

ASSOCIATED CONTENT

Supporting Information

The Supporting Information is available free of charge at <https://pubs.acs.org/doi/10.1021/acs.analchem.0c00929>.

Acoustic radiation pressure for a modulated standing wave; Tables S1–S8; Figures S1–S14; Supporting text: (A) Nonreactive mixing of ethanol and water; (B) Aqueous acetic acid and sodium hydroxycarbonate reaction; (C) Merging of a solid particle and a liquid droplet: water droplet and a copper sulfate crystal; Supporting references (PDF)

Movie S1 (MP4)

Movie S2 (MP4)

Movie S3 (MP4)

Movie S4 (MP4)

AUTHOR INFORMATION

Corresponding Author

Ralf I. Kaiser – Department of Chemistry, University of Hawaii at Manoa, Honolulu, Hawaii 96822, United States;
orcid.org/0000-0002-7233-7206; Email: ralfk@hawaii.edu

Author

Stephen J. Brotton – Department of Chemistry, University of Hawaii at Manoa, Honolulu, Hawaii 96822, United States;
orcid.org/0000-0002-8147-2960

Complete contact information is available at:
<https://pubs.acs.org/10.1021/acs.analchem.0c00929>

Author Contributions

R.I.K. and S.J.B. designed the experiment, discussed the experimental data, and wrote the manuscript. S.J.B. performed the experimental measurements.

Notes

The authors declare no competing financial interest.

ACKNOWLEDGMENTS

This work was supported by the Office of Naval Research under Grant N00014-16-1-2078. We thank Dr. E. G. Lierke for helpful discussions about the Tec5 acoustic levitator.

REFERENCES

- (1) Watanabe, A.; Hasegawa, K.; Abe, Y. *Sci. Rep.* **2018**, *8*, 10221.
- (2) Dagastine, R. R.; Manica, R.; Carnie, S. L.; Chan, D. Y. C.; Stevens, G. W.; Grieser, F. *Science* **2006**, *313*, 210–213.
- (3) Nikolopoulos, N.; Nikas, K. S.; Bergeles, G. *Comput. Fluids* **2009**, *38*, 1191–1202.
- (4) Shang, L. R.; Cheng, Y.; Zhao, Y. J. *Chem. Rev.* **2017**, *117*, 7964–8040.
- (5) Santesson, S.; Nilsson, S. *Anal. Bioanal. Chem.* **2004**, *378*, 1704–1709.
- (6) Kohno, J.; Higashiura, T.; Eguchi, T.; Miura, S.; Ogawa, M. *J. Phys. Chem. B* **2016**, *120*, 7696–7703.
- (7) Jacobs, M. I.; Davies, J. F.; Lee, L.; Davis, R. D.; Houle, F.; Wilson, K. R. *Anal. Chem.* **2017**, *89*, 12511–12519.
- (8) Ward, A. D.; Longhurst, M.; Quirke, N. *J. Exp. Nanosci.* **2006**, *1*, 75–82.
- (9) Lyuksyutov, I. F.; Naugle, D. G.; Rathnayaka, K. D. D. *Appl. Phys. Lett.* **2004**, *85*, 1817–1819.
- (10) King, L. V. *Proc. R. Soc. London A Mater.* **1934**, *147*, 212–240.
- (11) Gor'kov, L. P. *Sov. Phys. Doklady* **1962**, *6*, 773.
- (12) Yosioka, K.; Kawasima, Y. *Acta Acust. United Ac.* **1955**, *5*, 167–173.
- (13) Brotton, S. J.; Kaiser, R. I. *J. Phys. Chem. Lett.* **2013**, *4*, 669–673.
- (14) Brotton, S. J.; Kaiser, R. I. *Rev. Sci. Instrum.* **2013**, *84*, 055114.
- (15) Brotton, S. J.; Lucas, M.; Chambreau, S. D.; Vaghjiani, G. L.; Yu, J.; Anderson, S. L.; Kaiser, R. I. *J. Phys. Chem. Lett.* **2017**, *8*, 6053–6059.
- (16) Brotton, S. J.; Lucas, M.; Jensen, T. N.; Anderson, S. L.; Kaiser, R. I. *J. Phys. Chem. A* **2018**, *122*, 7351–7377.
- (17) Mason, N. J.; Drage, E. A.; Webb, S. M.; Dawes, A.; McPheat, R.; Hayes, G. *Faraday Discuss.* **2008**, *137*, 367–376.
- (18) Foresti, D.; Nabavi, M.; Klingauf, M.; Ferrari, A.; Poulikakos, D. *Proc. Natl. Acad. Sci. U. S. A.* **2013**, *110*, 12549–12554.
- (19) Andrade, M. A. B.; Camargo, T. S. A.; Marzo, A. *Rev. Sci. Instrum.* **2018**, *89*, 125105.
- (20) Bjelobrk, N.; Nabavi, M.; Poulikakos, D. *J. Appl. Phys.* **2012**, *112*, 053510.
- (21) Hamilton, M. F.; Blackstock, D. T. *Nonlinear Acoustics*; Academic Press: San Diego, CA, 1998; p xviii, 455 p.

- (22) Lucas, M.; Brotton, S. J.; Min, A.; Woodruff, C.; Pantoya, M. L.; Kaiser, R. I. *J. Phys. Chem. A* **2020**, *124*, 1489–1507.
- (23) Rothman, L. S.; Gordon, I. E.; Babikov, Y.; Barbe, A.; Benner, D. C.; et al. *J. Quant. Spectrosc. Radiat. Transfer* **2013**, *130*, 4–50.
- (24) Rayleigh, L. *Proc. R. Soc. London* **1879**, *29*, 71–97.
- (25) Shen, C. L.; Xie, W. J.; Wei, B. *Phys. Rev. E* **2010**, *81*, 046305.
- (26) Trinh, E. H.; Thiessen, D. B.; Holt, R. G. *J. Fluid Mech.* **1998**, *364*, 253–272.
- (27) Trinh, E.; Zwern, A.; Wang, T. G. *J. Fluid Mech.* **1982**, *115*, 453–474.
- (28) Trinh, E.; Wang, T. G. *J. Fluid Mech.* **1982**, *122*, 315–338.
- (29) Lierke, E. G.; Holitzner, L. *Meas. Sci. Technol.* **2008**, *19*, 115803.
- (30) Lierke, E. G. Acoustic Levitation - A brief memory update for insiders and Tec5 customers. *Technical note, Tec5 AG*; Oberursel, 2019.
- (31) Lierke, E. G. Reconsideration of axial and radial resonance oscillations of acoustically levitated drops or particles for a reliable concept. *Technical note, Tec5 AG*; Oberursel, 2015.
- (32) Cardulla, F. J. *Chem. Educ.* **1983**, *60*, 505–508.
- (33) Clark, J. D. *Ignition! An informal history of liquid rocket propellants*; Rutgers University Press: New Brunswick, N.J., 1972; p xiv, 214 p.
- (34) Schneider, S.; Hawkins, T.; Rosander, M.; Vaghjiani, G.; Chambreau, S.; Drake, G. *Energy Fuels* **2008**, *22*, 2871–2872.
- (35) Zhang, Y. Q.; Gao, H. X.; Joo, Y. H.; Shreeve, J. M. *Angew. Chem., Int. Ed.* **2011**, *50*, 9554–9562.
- (36) Schneider, S.; Hawkins, T.; Ahmed, Y.; Rosander, M.; Hudgens, L.; Mills, J. *Angew. Chem., Int. Ed.* **2011**, *50*, 5886–5888.
- (37) Zhang, Y. Q.; Shreeve, J. M. *Angew. Chem., Int. Ed.* **2011**, *50*, 935–937.
- (38) McCrary, P. D.; Chatel, G.; Alaniz, S. A.; Cojocar, O. A.; Beasley, P. A.; Flores, L. A.; Kelley, S. P.; Barber, P. S.; Rogers, R. D. *Energy Fuels* **2014**, *28*, 3460–3473.
- (39) Chambreau, S. D.; Koh, C. J.; Popolan-Vaida, D. M.; Gallegos, C. J.; Hooper, J. B.; Bedrov, D.; Vaghjiani, G. L.; Leone, S. R. *J. Phys. Chem. A* **2016**, *120*, 8011–8023.
- (40) Zhang, Q. H.; Shreeve, J. M. *Chem. Rev.* **2014**, *114*, 10527–10574.
- (41) McCrary, P. D.; Beasley, P. A.; Cojocar, O. A.; Schneider, S.; Hawkins, T. W.; et al. *Chem. Commun.* **2012**, *48*, 4311–4313.
- (42) McGraw, G. E.; Bernitt, D. L.; Hisatsune, I. C. *J. Chem. Phys.* **1965**, *42*, 237–244.
- (43) Minogue, N.; Riordan, E.; Sodeau, J. R. *J. Phys. Chem. A* **2003**, *107*, 4436–4444.
- (44) Socrates, G. *Infrared and Raman characteristic group frequencies: tables and charts*, 3rd ed.; Wiley: Chichester; New York, 2001; p xv, 347 p.
- (45) Wang, C. C.; Lang, E. K.; Signorell, R. *Astrophys. J., Lett.* **2010**, *712*, L40–L43.
- (46) Vasileiou, T.; Foresti, D.; Bayram, A.; Poulidakos, D.; Ferrari, A. *Sci. Rep.* **2016**, *6*, 20023.
- (47) Puskar, L.; Tuckermann, R.; Frosch, T.; Popp, J.; Ly, V.; McNaughton, D.; Wood, B. R. *Lab Chip* **2007**, *7*, 1125–1131.
- (48) Seinfeld, J. H. *Atmospheric chemistry and physics of air pollution*; Wiley: New York, 1986; p xxiii, 738 p.